Eddy compensation dampens Southern Ocean SST response to westerly wind trends

Edward W. Doddridge[1], John Marshall[1], Hajoon Song[1,2], Maxwell Kelley[3], and Larissa Nazarenko[3]

[1]Earth, Atmospheric and Planetary Science, Massachusetts Institute of Technology, 77 Massachusetts Avenue, Cambridge, 02139, USA

[2]Department of Atmospheric Sciences, Yonsei University, 134 Sinchon-dong, Seodaemun-gu, Seoul, 120-749, Korea

[3]NASA Goddard Institute for Space Studies, 2880 Broadway, New York, NY 10025 USA

Key Points:

- Antarctic circumpolar surface cooling is a robust response to enhanced westerly winds in models and observations
- Mesoscale eddy compensation prevents sustained upwelling of warm water beneath the seasonal ice zone (SIZ)
- Mesoscale eddy processes damp the response of the SIZ to enhanced westerly winds

Corresponding author: Edward W. Doddridge, `ewd@mit.edu`

Abstract

Anthropogenic influences have led to a strengthening and poleward shift of the westerly winds blowing over the Southern Ocean (SO), especially during the austral summer months. We use observations, an idealized high-resolution eddying-sea-ice channel model, and a global coupled climate model to explore the response of the SO to a step-change in the westerly wind. Previous work has hypothesized a two timescale response for sea surface temperature. Initially, horizontal Ekman transport away from Antarctica cools the surface before sustained upwelling of warm subsurface water leads to warming on decadal timescales. We find that the fast timescale response is robust across our two models and in accord with our analysis of observations: it consists of Ekman driven cooling in the mixed layer, warming at the temperature inversion due to anomalous upwelling, and warming in the seasonal thermocline due to enhanced vertical mixing. The long-term response is inaccessible from observations. However, neither of our models shows a long term subsurface warming. In our eddying channel this is a consequence of an eddy-driven circulation opposing the wind induced upwelling. This "eddy compensation" is also a feature of, although less pronounced in, our coupled climate model. Our results highlight the importance of accurately representing the mesoscale eddy contribution to the residual overturning circulation. We conclude that climate models which exhibit pronounced subsurface warming due to wind-induced upwelling are inconsistent with our understanding of SO dynamics and eddy compensation, and are unlikely to be able to capture the observed multi-decadal cooling SST trend around Antarctica.

1 Introduction

Over the satellite era the surface of the Southern Ocean around Antarctica has been observed to cool, in contrast to much of the rest of the earth's surface [see e.g. *Armour et al.*, 2016; *Marshall et al.*, 2015, and references therein]. There has also been a striking trend in the Southern Annular Mode (SAM) over the same period, with the SAM trending upwards [*Marshall*, 2003; *Jones et al.*, 2016], especially during the austral summer months of December, January, and February. Several modeling studies have suggested that the equilibrium response to a positive shift in the SAM is expected to be warming at the sea surface and a reduction in ice cover [*Bitz and Polvani*, 2012; *Sigmond and Fyfe*, 2010, 2013]. To reconcile the observed cooling and the modeled equilibrium warming *Ferreira et al.* [2015] and *Marshall et al.* [2014] proposed that the Southern Ocean responds to a step in the SAM on two distinct timescales; a rapid cooling, followed by a much slower warming trend. The mechanism behind this two-timescale response invokes surface Ekman transports to initially cool the sea surface, with Ekman upwelling eventually bringing warmer subsurface water, from below the wintertime mixed layer, up to the surface in the seasonal ice zone. Other recent studies have suggested additional processes that contribute to the formation of the cold SST anomaly, including atmospheric changes that alter the surface radiation budget [*Seviour et al.*, 2017a] and upwelling of cold water from the previous winter's mixed layer [*Purich et al.*, 2016].

Analysis of the models within the CMIP5 archive reveals substantial agreement on the initial cooling in response to a zonal wind change, but a range of long-term responses from continued cooling to rapid warming. The state of affairs is shown in Figure 1 a) adapted from *Kostov et al.* [2017, 2018]. *Kostov et al.* [2018] conclude that models which rapidly cross over from cooling to warming in response to a step change in the westerly winds are incompatible with the observed cooling of SST over the past 40 years, given the upward trending SAM over the same period. It should be noted that the historical simulations from the CMIP5 archive models underestimate the trend in westerly winds when compared with observations [*Purich et al.*, 2016]. While this should not bias the results of *Kostov et al.* [2017, 2018], since those analyses present temperature changes per unit change in the SAM, the underestimation of the westerly wind trend likely contributed to the inability of CMIP5 models to capture observed Antarctic sea ice trends [*Purich et al.*, 2016].

The long term subsurface warming trend discussed by *Ferreira et al.* [2015] is driven by an intensification of the Deacon Cell due to enhanced westerly winds. However, the expected long-term response of the SO overturning circulation to changes in wind stress is not a sustained strengthening of the Deacon Cell [see e.g. *Downes and Hogg*, 2013; *Gent*, 2016; *Marshall and Radko*, 2003; *Viebahn and Eden*, 2010]. It is instead the residual between an intensification of the wind-driven Deacon Cell and an opposing change in the eddy-driven circulation. The resulting change to the residual overturning circulation is expected to be much smaller than the initial perturbation to the Deacon Cell, and to have a different spatial structure. The horizontal resolution of CMIP5 models is too coarse to resolve mesoscale eddies, which must therefore be parameterized [*Gent and Mcwilliams*, 1990; *Gent et al.*, 1995]. Previous research has shown that mesoscale eddy effects are crucial for accurately simulating the behavior of the residual overturning circulation [*Downes* *and Hogg*, 2013; *Marshall and Radko*, 2003] and the strength of the Antarctic Circumpolar Current [*Munday et al.*, 2013]. Using a mesoscale eddy parameterization coefficient that varies in time and space substantially improves solutions of non-eddy-resolving ocean models, and perhaps how they respond to perturbations [*Danabasoglu and Marshall*, 2007; *Ferreira et al.*, 2005; *Gent*, 2016]. We might therefore expect that the response of ocean models to changes in the wind depends critically on whether they resolve the eddies responsible for the compensation or, if not, whether they have sufficiently skillful eddy parametrizations to faithfully simulate eddy compensation.

2 Observed response of the Southern Ocean to SAM

The expected short term response in the two timescale framework proposed by *Ferreira et al.* [2015] is a surface cooling and a warming at the temperature inversion[1] below the seasonal ice zone. Can we detect this signal in observations? Taking the average sea surface temperature (SST) between 55S and 70S from *Reynolds et al.* [2002], we can assess the short term response by comparing the DJF SST anomaly, Figure 1 b) blue line, and the DJF SAM value, Figure 1 b) orange line. Following *Marshall* [2003] the DJF SAM values are labeled for the year in which the December occurred. A linear regression of the DJF SAM values and the DJF SST yields a strong negative correlation (R^2 = 0.36, $p \approx 9 \times 10^{-5}$). This supports the idea that the initial response to a SAM is a surface cooling in the Southern Ocean close to Antarctica, as has been shown previously in observations [*Ciasto and Thompson*, 2008; *Doddridge and Marshall*, 2017] and modeling studies [*Ferreira et al.*, 2015; *Seviour et al.*, 2016, 2017a].

Using gridded data from the Argo array [*Roemmich and Gilson*, 2009] we can explore the initial zonal mean response to SAM anomalies below the surface of the Southern Ocean. However, there are several observational limitations that should be noted. Firstly, the gridded Argo dataset does not extend southwards into the seasonal ice zone, and so we are unable to assess the subsurface warming at the temperature inversion, which is a crucial component of the long timescale proposed by *Ferreira et al.* [2015]. Secondly, the time series is relatively short, which limits the statistical significance of the results. Despite these limitations, a regression analysis of zonal mean February temperatures from

[1] The temperature inversion is the region below the seasonal ice zone where $dT/dz < 0$, and hence upwelling leads to warming. This region is clearly visible in the temperature contours in the left hand side of Figure 1 c)

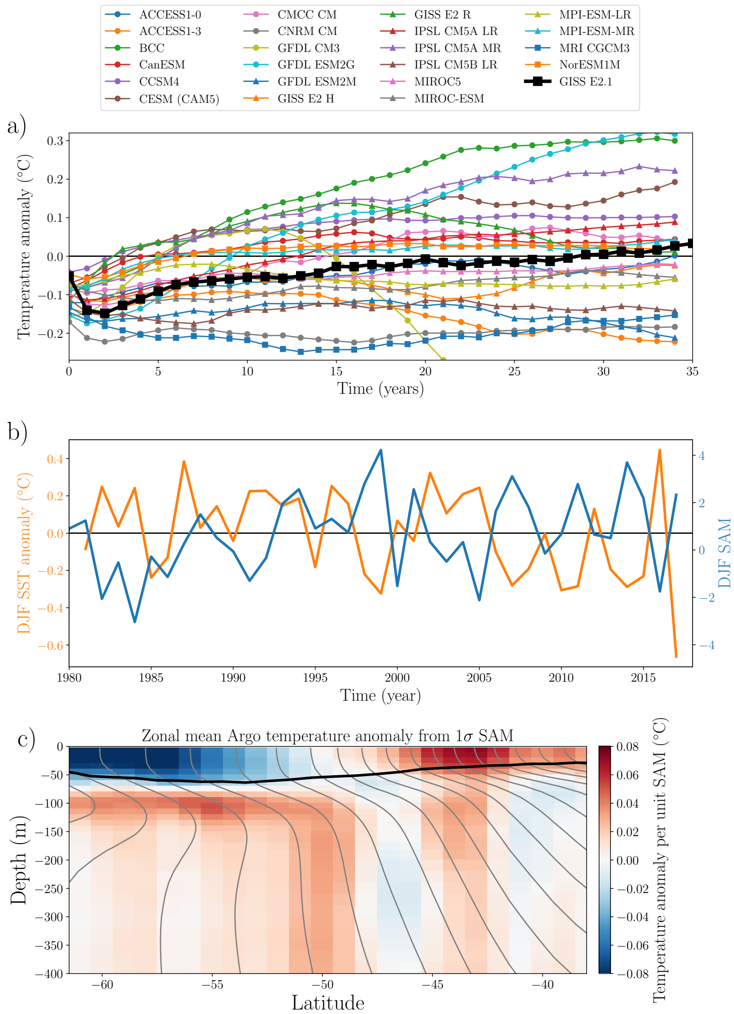

Figure 1. **a)** Climate response functions of the SST to a 1σ step change in the SAM index inferred from many different coupled CMIP5 climate models, modified from *Kostov et al.* [2017]. The response of the coupled model used here, developed at GISS and described in the supplementary information, is shown by the thick black line. **b)** DJF SAM time series from *Marshall* [2003] (blue line, right axis), and DJF sea surface temperature anomaly between 55S and 70S calculated from *Reynolds et al.* [2002] data (orange line, left axis). **c)** Zonal mean temperature anomaly in February due to a 1σ DJF SAM anomaly, estimated from gridded Argo data [*Roemmich and Gilson*, 2009] and a time series of observed SAM values [*Marshall*, 2003]. The black line is the climatological zonal mean mixed layer depth from *Holte et al.* [2017], and the gray contours show the zonal mean temperature field with a contour interval of 1°C.

the Argo dataset against the DJF SAM time series [*Marshall*, 2003] reveals a signal of cooling in the mixed layer and warming below, as shown in Figure 1 c). The vertical dipole in Figure 1 c) is centered just beneath the climatological February mixed layer depth from *Holte et al.* [2017], shown in black; this is consistent with the strengthened westerly winds enhancing mixing and deepening the mixed layer. This enhanced mixing moves heat downward through the water column, strengthening the cold anomaly in the mixed layer and warming the fluid below the mixed layer. This warming below the mixed layer is not part of the long term warming mechanism of *Ferreira et al.* [2015]. Rather, it is an as yet undescribed feature of the short term response. In later sections we will see that this vertical dipole is a robust feature across models, and show that it is caused by enhanced vertical mixing associated with stronger winds. The Argo data also reveal a reduction in salinity below the mean mixed layer depth (not shown); this is also consistent with enhanced vertical mixing drawing fresh water down from the surface.

3 Response of an eddying-ice ocean channel model to a step change in the westerly wind

We use a high resolution idealized eddy-resolving channel model to explore the importance of resolved mesoscale variability and eddy compensation in the response of the SO to a step change in the westerly wind. An overview of our idealized model is shown in Figure 2 and a more detailed description of the model configuration is given in the supplementary information. The model captures the dynamics of the seasonal ice zone and its interaction with a Circumpolar Current and its overturning cells. The domain is a reentrant channel 1200 km long and 3200 km wide. There is a continental shelf at the southern edge, and a flat bottom elsewhere in the domain. A sponge region at the northern boundary allows for a meridional overturning circulation. A meridional slice of the monthly mean CORE normal year forcings from 30 E is used for the external forcing fields. The meridional slice is tiled in the zonal direction to cover the entire domain, and hence there is no zonal variation in the surface forcings. The residual overturning streamfunction, shown in the outermost panel of Figure 2, exhibits both an upper cell and a lower cell, with the upwelling in the interior occurring along density surfaces, as expected [*Marshall and Speer*, 2012].

Once the channel model has reached a statistical equilibrium, we run two ensembles: a control ensemble using the same forcing as the spin up, and a perturbation ensemble in which the zonal wind speed, surface air temperature and specific humidity are altered in the austral summer months by the addition of a SAM-like anomaly. The perturbation is described in the supplementary information. We perturb the surface air temperature and

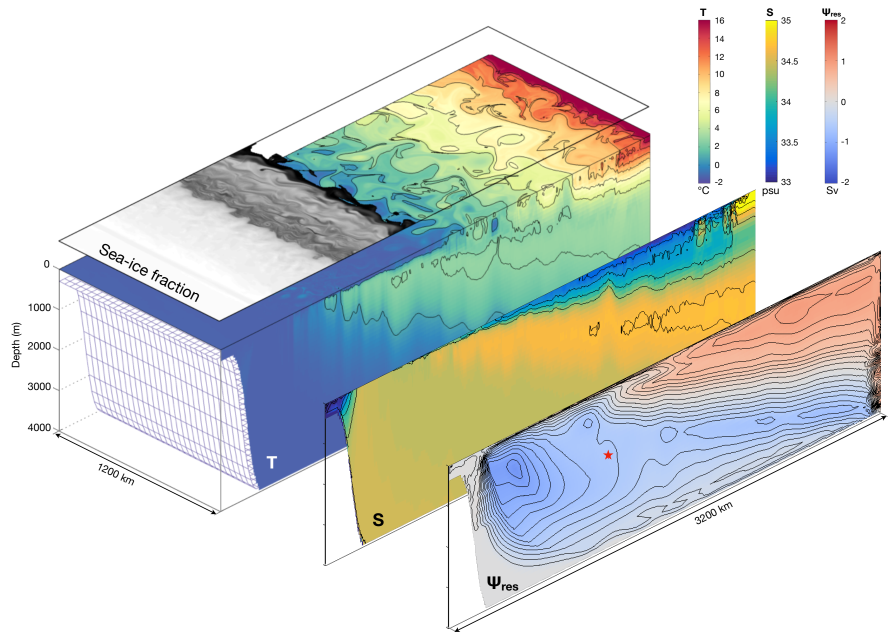

Figure 2. Overview of the idealized re-entrant channel eddying-ice control solution showing the instantaneous winter time sea ice concentration, temperature, and salinity fields, as well as the time-averaged residual overturning circulation. The model is driven by CORE normal year winds and fluxes. Note the presence of cold, fresh water at the surface in the region of the SIZ and a pronounced temperature inversion below. The red star denotes the position where a timeseries of residual-overturning strength in plotted in figure 3.

specific humidity so as to prevent unrealistic damping of SST anomalies after the application of the zonal wind perturbation; if these atmospheric fields are left unaltered then the SST anomaly decays much faster than observational estimates suggest is realistic [*Ciasto and Thompson*, 2008; *Doddridge and Marshall*, 2017; *Hausmann et al.*, 2016]. We find that four ensemble members are sufficient to obtain a robust response.

Above, we hypothesized that our eddy resolving model might not exhibit long term subsurface warming because the eddy-driven overturning circulation would spin up to compensate for the wind-driven change to the residual overturning circulation. The surface of our idealized channel model initially cools by approximately 0.05°C, as shown in Figure 3 a). While the magnitude of the SST anomaly decreases during the 10 year simulation, we do not see sustained long term warming. The initial cooling is consistent with that found in the CMIP5 models by *Kostov et al.* [2017]. Our model does not exhibit long term warming at the temperature inversion. The lack of a long term subsurface warming can be understood by considering the response of the residual overturning streamfunction. Figure 3 a) shows a time series of the anomalous residual overturning circulation extracted at the red star in the outermost panel of Figure 2. The star is located underneath the seasonal ice zone and ideally placed to provide an estimate of the anomalous upwelling responsible for the long warming predicted by *Ferreira et al.* [2015].

We find that the imposed wind anomaly initially strengthens the Deacon Cell and increases the upwelling through the temperature inversion, as shown in Figure 3 a) and b). However, within three years the eddy-driven overturning circulation strengthens to oppose this residual circulation change, as shown by the decrease in the overturning anomaly given by the black line in Figure 3 a). At equilibrium there is a relatively small net change in the residual overturning streamfunction at this location, see Figure 3 a). Such a rapid compensation timescale is consistent with previous estimates of the eddy spinup timescale from observations [*Meredith and Hogg*, 2006] and idealized models [*Screen et al.*, 2009; *Sinha and Abernathey*, 2016]. Without sustained upwelling through the temperature inversion the mechanism proposed by *Ferreira et al.* [2015] cannot lead to long term warming.

In addition to these anticipated responses, we also find a warm anomaly below the zonal mean mixed layer depth, as shown in Figure 3 b). This is very similar to the signal in the observations shown in Figure 1c. Heat budgets for the two rectangles in 3 b) are shown in c) and d). These indicate that the warming in the temperature inversion is due to enhanced upwelling as expected, while the warming below the mixed layer is due to enhanced vertical mixing. Further evidence for enhanced vertical mixing can be found in the salt distribution (not shown) and the mixed layer depth; the zonal mean mixed layer is consistently deeper in the perturbation ensemble than the control ensemble.

In summary we find that the initial response of the idealized channel model is consistent with the short timescale response proposed by *Ferreira et al.* [2015]: we see a cooling at the surface driven by horizontal Ekman transport, and a warming at the level of the temperature inversion due to enhanced upwelling. However, we do not observe the subsurface long-term warming hypothesized by *Ferreira et al.* [2015] because the residual overturning circulation required to create it rapidly (within a few years) damps away.

4 Response to a step ozone perturbation in a comprehensive coupled climate model

In this section we present results from simulations using the most recent NASA GISS coupled climate model, Model E2.1. Details of the model setup can be found in the supplementary information. From a long equilibrium pre-industrial control, we spawn perturbation experiments in which a seasonal hole in the stratospheric Antarctic ozone distribution is imposed to mimic conditions in the 1990s. Eight ensemble members are averaged to reduce the impact of internal variability. The ozone perturbation leads to a poleward shift of the jetstream, with enhanced summertime westerly winds around Antarctica and reduced westerlies further north. The upper panel of Figure 4 a) shows the climatological zonal wind (contours) and anomalies reaching down to the surface (colors). This enhancement of westerly winds during the austral summer is a well known consequence of stratospheric ozone depletion [see e.g. *Gerber and Son*, 2014; *Polvani et al.*, 2011; *Seviour et al.*, 2017b]. What happens in the underlying ocean?

The strengthened surface westerly winds initially cause cold SST anomalies through enhanced equatorward Ekman transport in the underlying ocean. A time series of the SST anomalies is shown by the orange line in Figure 4 b). We also observe anomalous upwelling due to a Deacon Cell-like perturbation to the residual overturning circulation. A time series of the anomalous overturning streamfunction is shown by the black line in Figure 4 b). Note that there is considerably more variability in these fields compared to the channel model, even though twice as many ensemble members were averaged. This is because of internal variability in the coupled model that is not present in the ocean-only model despite the presence of intense mesoscale variability in the latter. Note that the anomalous residual overturning circulation decays away over time, on the same time-scale as that of the SST and inversion temperature anomaly, all three exhibiting synchronous oscillations. Beyond 15 years or so natural variability of the coupled system dominates, the amplitude of which is indicated by the vertical gray bar in figure 4 b).

Figure 4 c) shows the vertical structure of the temperature anomalies in February of the second year of the simulation. We see a vertical cooling-warming dipole centered on the mixed layer depth, and a weak warming in the temperature inversion, which is strikingly similar to that found in the channel model in Figure 3 b) and in the observations, Figure 1 c). Much as in the eddying channel model, the warm anomaly at the level of the temperature inversion does not grow substantially during the first 20 years of the perturbation, see the green line in Figure 4 b). After 20 years the temperature anomaly at the inversion does increase, but anomalous upwelling cannot be the causal mechanism since the overturning anomaly is small by this time, see blue line in Figure 4 b). As discussed previously, the initial SST response reveals a cooling, but the long term evolution of SST is less clear. Despite analyzing an ensemble of simulations the presences of internal variability with a magnitude of approximately 0.1 K from year 15 onwards makes it difficult to identify whether a warming trend is present in the latter part of the time series. Taking an average of the SST anomaly between years 20 and 40 shows a small warming, consistent with the climate response function shown in Figure 1 a). Despite the variability in the latter part of the time series, the lack of warming at the temperature inversion during the time period with anomalous upwelling rules out the mechanism proposed by *Ferreira et al.* [2015] as a source of any long term warming in this model.

We conclude that, just as in the eddying channel model, the GISS coupled model does not exhibit a pronounced warming trend, either at the surface or at depth. This is consistent with the SST CRF deduced (by lagged regression between SAM and SST) from a long control run of the GISS model shown by the thick black line in Figure 1c. The cross-over from cooling to warming is barely evident, even after 30 years.

5 Discussion and Conclusions

Ferreira et al. [2015] proposed a two timescale mechanism drawing together observational evidence that strengthening westerly winds were associated with a cooling of the sea surface and an expansion of sea ice, and modeling evidence that suggested stratospheric ozone depletion would eventually lead to warmer SSTs and a loss of sea ice. However, the mechanism proposed by *Ferreira et al.* [2015] relies on a persistent intensification of the Deacon Cell and a growing subsurface temperature anomaly that is eventually entrained into the mixed layer thereby warming the sea surface. While we are unable to address the long term changes from observations, we do not find this mechanism at work in either of our numerical experiments. Instead, we see a transient intensification of the Deacon Cell, which then fades and does not lead to subsurface warming below the seasonal ice zone. While atmospheric processes may also be important, as suggested by *Seviour et al.* [2017a], the mechanism we have focused on here is an oceanic one, and we find no evidence of a subsurface warming driven by anomalous upwelling. Instead, we find that anomalous upwelling fades over time.

The initial response to strengthened westerly winds is consistent between the observations, an idealized eddying ocean sea-ice model, and a global coupled model. In each of these cases we observe a vertical cooling-warming dipole centered on the zonal mean mixed layer depth. The warming just below the mixed layer is driven by anomalous vertical mixing and is unrelated to the mechanism proposed by *Ferreira et al.* [2015]. The observations and the coupled model also show a warming to the north, in the region where the westerly winds weaken due to a poleward shift in the atmospheric jet.

The long timescale is inaccessible from observations but can be addressed in our models. In both we initially find a small warming at the temperature inversion under the seasonal ice zone. However, this anomaly does not continue to grow, and the models do not exhibit persistent anomalous upwelling in this region. In our idealized channel model, the lack of persistent upwelling is due to a change in the eddy-driven overturning circulation which compensates for the altered wind-driven overturning; a process known as eddy compensation [see e.g. *Downes and Hogg*, 2013; *Gent*, 2016; *Viebahn and Eden*, 2010]. Since the GISS model is a complex global coupled model, the lack of substantial long-term warming could be due to many different physical processes. We can however say that the anomalous overturning circulation induced by the ozone hole decays away over time and does not lead to subsurface warming in the seasonal ice zone.

The global coupled model includes a parameterization for mesoscale eddies that relates the slope of the isopycnals to the strength of the eddy-induced overturning circulation. In the simplest parameterizations, where κ_{GM} is a monolithic constant, the strength of the eddy-induced circulation is directly proportional to the slope. The parameterization used by GISS Model version 2.1 dynamically assigns κ_{GM} based on the flow and isopycnal slope. This means that the strength of the eddy-induced overturning circulation is proportional to the isopycnal slop raised to the power n, where $2 \leq n \leq 3$ (see supplemental information for details of the parameterization). Since the eddy-induced overturning depends on the isopycnal slope raised to some power, small changes in the slope produce relatively large changes in the eddy-induced overturning circulation. This sensitivity helps to prevent wind perturbations causing large changes to the isopycnal slopes; a process known as eddy compensation.

Our results contrast with those of *Bitz and Polvani* [2012] who found that their eddy-resolving coupled-climate model did warm in response to an ozone perturbation. But, figure 3 in *Bitz and Polvani* [2012] shows that the zonal mean ocean warming does not occur near the temperature inversion. Rather, they find warming further north, and attribute it anomalous downwelling. However, it should be noted that their figure 4 shows the Eulerian-mean overturning, rather than the more pertinent residual overturning circulation [*Marshall and Radko*, 2003].

Finally, it should be noted that *Kostov et al.* [2018] show that CMIP5 models have a wide range of responses to a step change in the SAM. They conclude that models which exhibit strong warming are incompatible with the observational record. Furthermore, long term warming caused by a persistent intensification of the Deacon Cell, as hypothesized by *Ferreira et al.* [2015], is inconsistent with our current understanding of SO dynamics. Here we have presented two numerical simulations that do not exhibit long term warming and shown that this is related to a reduction in anomalous upwelling. Our results lend support to the conclusions of *Kostov et al.* [2018] and identify an important ocean mechanism at work that damps the response of the SIZ to anomalous winds.

Acknowledgments

EWD acknowledges support from the NSF's FESD program. JM acknowledges support from the MIT-GISS collaborative agreement and the NSF Polar Antarctic Program.

We are grateful to Douglas Kinnison for assitance with the ozone perturbation for the GISS simulations. The National Center for Atmospheric Research (NCAR) is sponsored by the U.S. National Science Foundation (NSF). WACCM is a component of NCAR's Community Earth System Model (CESM), which is supported by the NSF and the Office of Science of the U.S. Department of Energy. Computing resources were provided by NCAR's Climate Simulation Laboratory, sponsored by NSF and other agencies. This research was enabled by the computational and storage resources of NCAR's Computational and Information Systems Laboratory (CISL). The WACCM model output and data used in this paper are listed in the references or available from the NCAR Earth System Grid.

References

Armour, K. C., J. C. Marshall, J. R. Scott, A. Donohoe, and E. R. Newsom (2016), Southern Ocean warming delayed by circumpolar upwelling and equatorward transport, *Nat. Geosci.*, *9*(7), 549–554, doi:10.1038/ngeo2731.

Bitz, C. M., and L. M. Polvani (2012), Antarctic climate response to stratospheric ozone depletion in a fine resolution ocean climate model, *Geophys. Res. Lett.*, *39*(20), 1–5, doi: 10.1029/2012GL053393.

Ciasto, L. M., and D. W. J. Thompson (2008), Observations of large-scale ocean-atmosphere interaction in the Southern Hemisphere, *J. Clim.*, *21*(6), 1244–1259, doi: 10.1175/2007JCLI1809.1.

Danabasoglu, G., and J. C. Marshall (2007), Effects of vertical variations of thickness diffusivity in an ocean general circulation model, *Ocean Model.*, *18*(2), 122–141, doi: 10.1016/j.ocemod.2007.03.006.

Doddridge, E. W., and J. C. Marshall (2017), Modulation of the Seasonal Cycle of Antarctic Sea Ice Extent Related to the Southern Annular Mode, *Geophys. Res. Lett.*, *44*(19), 9761–9768, doi:10.1002/2017GL074319.

Downes, S. M., and A. M. C. C. Hogg (2013), Southern Ocean Circulation and Eddy Compensation in CMIP5 Models, *J. Clim.*, *26*(18), 7198–7220, doi:10.1175/JCLI-D-12-00504.1.

Ferreira, D., J. C. Marshall, and P. Heimbach (2005), Estimating Eddy Stresses by Fitting Dynamics to Observations Using a Residual-Mean Ocean Circulation Model and Its Adjoint, *J. Phys. Oceanogr.*, *35*(10), 1891–1910, doi:10.1175/JPO2785.1.

Ferreira, D., J. C. Marshall, C. M. Bitz, S. Solomon, and A. Plumb (2015), Antarctic ocean and sea ice response to ozone depletion: A two-time-scale problem, *J. Clim.*, *28*(3), 1206–1226, doi:10.1175/JCLI-D-14-00313.1.

Gent, P. R. (2016), Effects of Southern Hemisphere Wind Changes on the Meridional Overturning Circulation in Ocean Models, *Ann. Rev. Mar. Sci.*, *8*(1), 79–94, doi: 10.1146/annurev-marine-122414-033929.

Gent, P. R., and J. C. Mcwilliams (1990), Isopycnal Mixing in Ocean Circulation Models, *J. Phys. Oceanogr.*, *20*(1), 150–155, doi:10.1175/1520-0485(1990)020<0150:IMIOCM>2.0.CO;2.

Gent, P. R., J. Willebrand, T. J. McDougall, and J. C. McWilliams (1995), Parameterizing Eddy-Induced Tracer Transports in Ocean Circulation Models, *J. Phys. Oceanogr.*, *25*(4), 463–474, doi:10.1175/1520-0485(1995)025<0463:PEITTI>2.0.CO;2.

Gerber, E. P., and S. W. Son (2014), Quantifying the summertime response of the Austral jet stream and hadley cell to stratospheric ozone and greenhouse gases, *J. Clim.*, *27*(14), 5538–5559, doi:10.1175/JCLI-D-13-00539.1.

Hausmann, U., A. Czaja, and J. C. Marshall (2016), Estimates of Air-Sea Feedbacks on Sea Surface Temperature Anomalies in the Southern Ocean, *J. Clim.*, *29*(2), 439–454, doi:10.1175/JCLI-D-15-0015.1.

Holte, J., L. D. Talley, J. Gilson, and D. Roemmich (2017), An Argo mixed layer climatology and database, *Geophys. Res. Lett.*, *44*(11), 5618–5626, doi:10.1002/2017GL073426.

Jones, J. M., S. T. Gille, H. Goosse, N. J. Abram, P. O. Canziani, D. J. Charman, K. R. Clem, X. Crosta, C. de Lavergne, I. Eisenman, M. H. England, R. L. Fogt, L. M. Frankcombe, G. J. Marshall, V. Masson-Delmotte, A. K. Morrison, A. J. Orsi, M. N. Raphael, J. A. Renwick, D. P. Schneider, G. R. Simpkins, E. J. Steig, B. Stenni, D. Swingedouw, and T. R. Vance (2016), Assessing recent trends in high-latitude Southern Hemisphere surface climate, *Nat. Clim. Chang.*, *6*(10), 917–926, doi:10.1038/nclimate3103.

Kostov, Y., J. C. Marshall, U. Hausmann, K. C. Armour, D. Ferreira, and M. M. Holland (2017), Fast and slow responses of Southern Ocean sea surface temperature to SAM in coupled climate models, *Clim. Dyn.*, *48*(5-6), 1595–1609, doi:10.1007/s00382-016-3162-z.

Kostov, Y., D. Ferreira, K. C. Armour, and J. C. Marshall (2018), Contributions of greenhouse gas forcing and the Southern Annular Mode to historical Southern Ocean surface temperature trends, *Geophys. Res. Lett.*, doi:10.1002/2017GL074964.

Marshall, G. J. (2003), Trends in the Southern Annular Mode from Observations and Reanalyses, *J. Clim.*, *16*(24), 4134–4143, doi:10.1175/1520-0442(2003)016<4134:TITSAM>2.0.CO;2.

Marshall, J. C., and T. Radko (2003), Residual-Mean Solutions for the Antarctic Circumpolar Current and Its Associated Overturning Circulation, *J. Phys. Oceanogr.*, *33*(11), 2341–2354, doi:10.1175/1520-0485(2003)033<2341:RSFTAC>2.0.CO;2.

Marshall, J. C., and K. Speer (2012), Closure of the meridional overturning circulation through Southern Ocean upwelling, *Nat. Geosci.*, *5*, doi:10.1038/NGEO1391.

Marshall, J. C., K. C. Armour, J. R. Scott, Y. Kostov, U. Hausmann, D. Ferreira, T. G. Shepherd, and C. M. Bitz (2014), The ocean's role in polar climate change: asymmetric Arctic and Antarctic responses to greenhouse gas and ozone forcing, *Philos. Trans. R. Soc. A Math. Phys. Eng. Sci.*, *372*(2019), 20130,040–20130,040, doi:10.1098/rsta.2013.0040.

Marshall, J. C., J. R. Scott, K. C. Armour, J.-M. Campin, M. Kelley, and A. Romanou (2015), The ocean's role in the transient response of climate to abrupt greenhouse gas forcing, *Clim. Dyn.*, *44*(7-8), 2287–2299, doi:10.1007/s00382-014-2308-0.

Meredith, M. P., and A. M. Hogg (2006), Circumpolar response of Southern Ocean eddy activity to a change in the Southern Annular Mode, *Geophys. Res. Lett.*, *33*(16), 2–5, doi:10.1029/2006GL026499.

Munday, D. R., H. L. Johnson, and D. P. Marshall (2013), Eddy Saturation of Equilibrated Circumpolar Currents, *J. Phys. Oceanogr.*, *43*(3), 507–532, doi:10.1175/JPO-D-12-095.1.

Polvani, L. M., D. W. Waugh, G. J. P. Correa, and S.-W. Son (2011), Stratospheric Ozone Depletion: The Main Driver of Twentieth-Century Atmospheric Circulation Changes in the Southern Hemisphere, *J. Clim.*, *24*(3), 795–812, doi:10.1175/2010JCLI3772.1.

Purich, A., W. Cai, M. H. England, and T. Cowan (2016), Evidence for link between modelled trends in Antarctic sea ice and underestimated westerly wind changes, *Nat. Commun.*, *7*, 10,409, doi:10.1038/ncomms10409.

Reynolds, R. W., N. A. Rayner, T. M. Smith, D. C. Stokes, and W. Wang (2002), An improved in situ and satellite SST analysis for climate, *J. Clim.*, *15*(13), 1609–1625, doi: 10.1175/1520-0442(2002)015<1609:AIISAS>2.0.CO;2.

Roemmich, D., and J. Gilson (2009), The 2004-2008 mean and annual cycle of temperature, salinity, and steric height in the global ocean from the Argo Program, *Prog. Oceanogr.*, *82*(2), 81–100, doi:10.1016/j.pocean.2009.03.004.

Screen, J. A., N. P. Gillet, D. P. Stevens, G. J. Marshall, and H. K. Roscoe (2009), The role of eddies in the Southern Ocean temperature response to the southern annular mode, *J. Clim.*, *22*(3), 806–818, doi:10.1175/2008JCLI2416.1.

Seviour, W. J., A. Gnanadesikan, D. Waugh, and M. A. Pradal (2017a), Transient response of the Southern Ocean to changing ozone: Regional responses and physical mechanisms, *J. Clim.*, *30*(7), 2463–2480, doi:10.1175/JCLI-D-16-0474.1.

Seviour, W. J., D. W. Waugh, L. M. Polvani, G. J. Correa, and C. I. Garfinkel (2017b), Robustness of the simulated tropospheric response to ozone depletion, *J. Clim.*, *30*(7), 2577–2585, doi:10.1175/JCLI-D-16-0817.1.

Seviour, W. J. M., A. Gnanadesikan, and D. W. Waugh (2016), The Transient Response of the Southern Ocean to Stratospheric Ozone Depletion, *J. Clim.*, *29*(20), 7383–7396, doi:10.1175/JCLI-D-16-0198.1.

Sigmond, M., and J. C. Fyfe (2010), Has the ozone hole contributed to increased Antarctic sea ice extent?, *Geophys. Res. Lett.*, *37*(18), doi:10.1029/2010GL044301.

Sigmond, M., and J. C. Fyfe (2013), The Antarctic Sea Ice Response to the Ozone Hole in Climate Models, *J. Clim.*, *27*, 1336–1342, doi:10.1175/JCLI-D-13-00590.1.

Sinha, A., and R. P. Abernathey (2016), Time Scales of Southern Ocean Eddy Equilibration, *J. Phys. Oceanogr.*, *46*(9), 2785–2805, doi:10.1175/JPO-D-16-0041.1.

Viebahn, J., and C. Eden (2010), Towards the impact of eddies on the response of the Southern Ocean to climate change, *Ocean Model.*, *34*(3-4), 150–165, doi:10.1016/j.ocemod.2010.05.005.

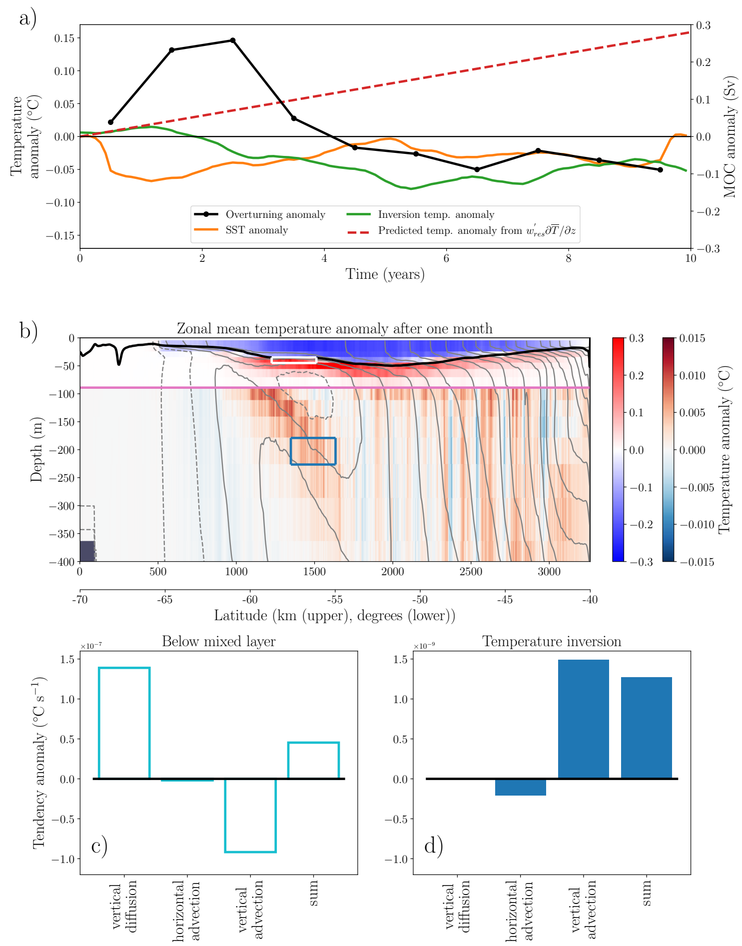

Figure 3. **a)** Time series of anomalous residual overturning circulation at the red "star" shown in figure 2 (black line, right axis), the average SST anomaly between y = 500 and 2500 km (orange line), the inversion temperature anomaly at 179 m depth between y = 1200 and 1600 km (green line), and the predicted inversion temperature anomaly calculated using the average anomalous upwelling in the first two years and the vertical temperature gradient (dashed red line). The temperature scale is shown on the left hand axis, and both temperature time series have been smoothed with 12 month running means. **b)** zonal mean temperature anomaly after one month of perturbed forcing (colors, note the change in color scale at the horizontal pink line at 90 m depth), the light gray contours show the climatological model temperature field in February (1°C contour interval, negative contours dashed), and the thick black line shows the zonal mean mixed layer depth from the perturbation ensemble. **c)** and **d)** heat budgets showing that the anomalous warming below the mixed layer is due to enhanced vertical mixing, while the warming at the temperature inversion is due to enhanced upwelling. The colors of the bar plots are matched to the rectangles shown in b). The contribution from horizontal mixing is negligible, and thus not shown. Note the different vertical scales in c) and d).

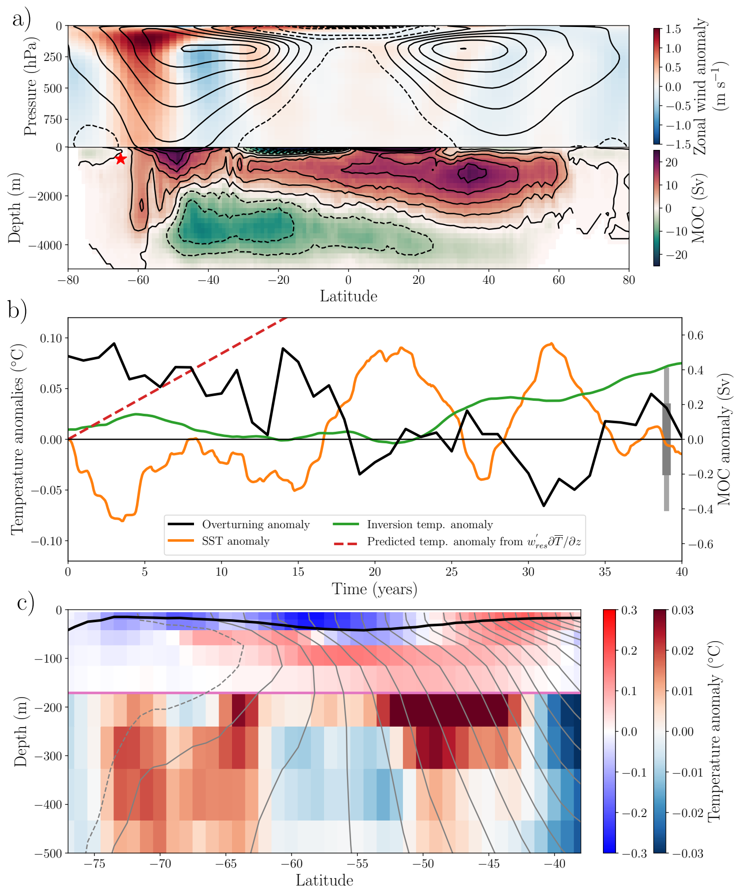

Figure 4. **a)** Upper panel: zonal mean zonal wind in January (contours with 5 ms^{-1} contour interval, zero and negative contours dashed) and zonal mean zonal wind anomalies due to ozone perturbation (colors). Lower panel: time-averaged residual overturning circulation from the control simulation. **b)** time series of the anomalous residual overturning circulation (blue line, right axis) extracted at the red star in a) located at 65 S and 492 m depth. Time series of the anomalous temperature at the temperature inversion (73-63 S, 328 m depth, green line), the SST anomaly (70-55 S, orange line), and the anticipated temperature anomaly at the inversion calculated from the average anomalous upwelling and vertical temperature gradient (dashed red line), with temperature scale shown on the left hand axis. All lines represent ensemble means and have been smoothed with a five year running mean. The thin and thick gray vertical shaded regions show the variability of the control ensemble SST and represent 1σ and 2σ respectively. **c)** zonal mean temperature anomaly (colors) in February of the second year of the simulation, and the climatological temperature in February from the control ensemble (gray contours, contour interval 1°C, negative contours dashed). The vertical dipole of cooling and warming centered on the mixed layer depth can be clearly seen, as can the warming at the temperature inversion. The zonal mean mixed layer depth from the perturbation ensemble is shown by the black line. Note the change in color scale either side of the horizontal pink line at 171 m depth.

Supporting Information for
"Eddy compensation dampens Southern Ocean SST response to westerly wind trends"

Edward W. Doddridge[1], John Marshall[1], Hajoon Song[1,2], Maxwell Kelley[3], and Larissa Nazarenko[3]

[1]Earth, Atmospheric and Planetary Science, Massachusetts Institute of Technology, 77 Massachusetts Avenue, Cambridge, 02139, USA

[2]Department of Atmospheric Sciences, Yonsei University, 134 Sinchon-dong, Seodaemun-gu, Seoul, 120-749, Korea

[3]NASA Goddard Institute for Space Studies, 2880 Broadway, New York, NY 10025 USA

Contents

Text S1.

An eddy-rich channel model is prepared using MIT general circulation model (MITgcm) [*Marshall et al.*, 1997b,a; *Adcroft et al.*, 1997; *Marshall et al.*, 1998] to represent the Southern Ocean and the ACC. The domain has a size of 1200 km by 3200 km in zonal and meridional directions respectively, with 4 km horizontal resolution. There are 50 vertical levels from the surface to 4000 m. The top 50 m is resolved at every 10 m, and the intervals between levels increases to 100 m towards the bottom. There is a 300 m deep, 80 km wide shelf near the southern boundary that drops to the bottom within 300 km of the southern boundary.

Temperature and salinity from the World Ocean Atlas version 2 [*Locarnini et al.*, 2013; *Zweng et al.*, 2013] along 30°E were extended zonally within the model domain and used to initialize the model. The east and west boundaries are connected; when fluid

Corresponding author: Edward W. Doddridge, `ewd@mit.edu`

leaves from one side, it re-enters from the other. The northern and southern boundaries are closed, although there is an approximately 100 km wide sponge layer at the northern boundary where temperature and salinity are relaxed to the initial conditions with a 10 day timescale. This sponge region allows for the presence of a meridional overturning circulation within the model domain.

A sea-ice model is coupled to the MITgcm to simulate the change of the sea-ice properties such as concentration, thickness and velocity. The thermodynamics of the sea-ice model is based on the formulation by *Winton* [2000] where the sea-ice and snow thickness are calculated using heat fluxes from the top and bottom surfaces. The sea-ice dynamics is based on the elastic-viscous-plastic method by *Hunke and Dukowicz* [1997] where both atmospheric, oceanic and internal stresses drive the sea-ice movement. A detailed description of the sea-ice model can be found in *Losch et al.* [2010]. The sea-ice model was initialized with 1 m thick layer of sea-ice covering everywhere south of 56°S.

The ocean in the channel was forced by monthly mean atmospheric data from the Corrected Normal Year Forcing Version 2.0 product [*Large and Yeager*, 2009] through bulk formulae [*Large and Pond*, 1982]. As with the initial conditions, the values along 30°E were extended to cover the channel, so there is no zonal variation in surface forcing. The model was then integrated for 50 model years with the vertical mixing computed with the turbulent kinetic energy scheme by *Gaspar et al.* [1990] by which time the model reaches a quasi-equilibrium. Upon reaching a quasi-equilibrium, perturbation experiments are initiated in January by modifying the imposed atmospheric fields.

Tracer distributions

One of the important characteristics observed near the seasonal sea-ice zone is the temperature inversion; cold and fresh water sits above warm and salty water and insulates sea-ice from the warmth below. Our model reproduces this temperature inversion in the near surface ocean (figure S1(a)). The mass of warm (above 0°C) and salty (salinity greater than 34.7 psu) water reaches well beyond the winter time ice edge, and finishes close to 65°S. The upwelling branch of both overturning cells is responsible for the delivery of this water-mass (figure S2). The presence of a temperature inversion indicates that salinity dominates the density field in this region.

The water-mass on the shelf is very fresh (< 34 psu) and light when compared with the water further offshore (figure S1(b)), resulting in a strong horizontal density gradient. As might be anticipated from thermal wind, we see a strong westward zonal flow in this region. To the north of 67°S, the density decreases with the latitude, and the zonal flow is eastward (figure S1(c)).

Overturning circulations

The channel model reproduces the two-cell structure well (figure S2). The upper cell and lower cell separate close to the location of zero zonal wind stress, where the meridional Ekman transports diverge (figure S2. Fluid upwells along the the interface between the two cells (Figure S2); this is what supplies the warm salty water to the subsurface in the seasonal ice zone. At the surface, the upper cell moves fluid equatorwards while the lower cell transports waters toward the pole. The subduction of dense water in the lower cell occurs near 67°S and sets the abyssal water properties of our model.

Imposed atmospheric anomalies

We mimic the effect of an increasingly positive Southern Annular Mode by imposing zonal wind speed, surface humidity, and surface temperature anomalies in the austral summer months. The use of specified atmospheric fields is equivalent to an atmosphere with an infinite heat capacity, which means that the atmosphere-ocean fluxes are too large if the temperature and humidity fields are left unmodified. The control and perturbed versions of surface temperature, specific humidity, and zonal wind speed from January are shown in figure S3.

Text S2

This study employs GISS modelE version 2.1 (E2.1) in a configuration retaining the same horizontal and vertical resolutions as the version 2 described by *Schmidt et al.* [2014]. The atmospheric component is on a 2x2.5 degree latitude-longitude grid with 40 layers and a top at 0.1 hPa. The sea ice component is on the atmospheric grid. The ocean component is on a 1x1.25 degree latitude-longitude grid with 32 mass layers down to 4990 m; the nominal depths of the top 8 layer interfaces are at 12, 30, 56, 92, 140, 202, 280, and 376 m.

E2.1 features numerous updates to physical parameterizations and numerics which will be described as part of the documentation of GISS submissions to CMIP6. Primarily due to improvements to the ocean mesoscale scheme, its Southern Ocean climatology is significantly better than that of E2, which suffered from weak stratification and too little sea ice. The representation of eddy-induced circulation employs a Gent-McWilliams form [*Gent and Mcwilliams*, 1990; *Gent et al.*, 1995], with a three-dimensional diffusivity equal to that for isoneutral mixing of tracers [*Redi*, 1982]. This diffusivity K_{meso} has an interactive local dependence on the magnitude of density gradients, as well as their vertical structure: $K_{meso} = K_0 PR$. The surface diffusivity K_0 follows *Visbeck et al.* [1997] in its use of the spatially varying Eady growth rate but has been simplified to use a constant horizontal length scale (J. Marshall, pers. comm.):

$$K_0 = C(T_{eady})^{-1}, \tag{1}$$

where $C = (38.7km)^2$ and $(T_{eady})^{-1} = \{|sN|\}$, where s is the slope of neutral surfaces, N is the Brunt-Vaisala frequency, and $\{\}$ denotes averaging over the upper D meters of ocean depth. D is calculated as

$$D = min(max(z_{bot}, 400m), 1000m), \tag{2}$$

where z_{bot} is the local ocean depth. This means that the average is always taken over at least 400 m. When z_{bot} is less than 400 m, the product sN is assumed to be zero between 400 m and z_{bot}.

Vertical variation in the strength of the parametrized eddies in introduced through the non-dimensional profile factor $P = e^{-z/z_{scale}}$, which represents the surface intensification of eddy activity. The vertical scale characterizes the depth over which surface-connected eddies are active, and is calculated as

$$z_{scale} = \frac{[|\rho_h z|]}{[|\rho_h|]}, \tag{3}$$

in which [] denotes vertical integration from $min(z_{bot}, 3000m)$ to the surface, and ρ_h is the horizontal gradient of density. A qualitative representation of the enhancement of eddy diffusivity at low latitudes (due to the larger Rossby radius and length scales there) is included via $R = 1/max(0.1, sin(|latitude|))$. The eddy-induced streamfunction (not shown) has its largest magnitude and is deepest in the Southern Ocean, mostly canceling the Deacon cell. Mainly by analogy to this climatological eddy compensation, we believe that the parametrized eddy response to a wind-perturbation tilting of high-latitude isopycnals is a negative feedback. The interactivity of the eddy diffusivity was designed for its ability to distinguish the Southern Ocean regime (slowly decaying P, large K_0) from other basins and did not target apparent eddy compensation timescales there. The appearance of a factor of s in K_0 causes the eddy-induced streamfunction $\Psi = K_{meso}s$ to depend on s to the second power, and the dependence of P on ρ_h likely further increases the exponent.

The ocean employs the KPP scheme for vertical mixing, with the addition of a diffusivity associated with tidal dissipation near the seafloor. Mixed-layer depths in the Southern Ocean compare reasonably well to observations, peaking in the core of the ACC.

Prescription of the ozone hole in E2.1

A separate atmospheric chemistry model was used to create ozone fields for the GISS E2.1 simulations. The Community Earth System Model version 1 (CESM1), Whole Atmosphere Community Climate Model (WACCM), is a chemistry climate model from the Earth's surface to the lower thermosphere [*Garcia et al.*, 2007; *Kinnison et al.*, 2007; *Marsh et al.*, 2013] . WACCM is superset of the Community Atmosphere Model, version 4 (CAM4), and includes all of the physical parameterizations of CAM4 [*Neale et al.*, 2013] and a finite volume dynamical core [*Lin*, 2004] for the tracer advection. The horizontal resolution is 1.9° latitude x 2.5° longitude. The vertical resolution in the lower stratosphere ranges from 1.2 km near the tropopause to about 2 km near the stratopause; in the mesosphere and thermosphere the vertical resolution is 3km. The version of CESM1 (WACCM) used in this work was updated for the Chemistry Climate Model Initiative (CCMI) assessment [*Morgenstern et al.*, 2017]. Improvements in CESM1 (WACCM) for CCMI includes a modification to the orographic gravity wave forcing that reduced the cold bias in Antarctic polar temperatures [*Garcia et al.*, 2017] and updates to the stratospheric heterogeneous chemistry which improved the representation of polar ozone depletion [*Solomon et al.*, 2015]. In this work, there are two scenarios examined which span the pre-industrial, 1850s period and the near present-day, 1995-2001 period. Both scenarios include forcing of greenhouse gases (CH4, N2O, and CO2), organic halogens, volcanic surface area density and heating, and 11-year solar cycle variability for their respective periods. In the pre-industrial period, a representation of the QBO is included as described in *Marsh et al.* [2013]. The sea surface temperatures are based on observations (i.e., this version is not coupled to an interactive ocean). The 1995-2001 period uses the specified dynamics (SD) option in WACCM [*Lamarque et al.*, 2012]. Here, temperature, zonal and meridional winds, and surface pressure are used to drive the physical parameterization that control boundary layer exchanges, advective and convective transport, and the hydrological cycle. The meteorological analyses are taken from the National Aeronautics and Space Administration (NASA) Global Modeling and Assimilation Office (GMAO) Modern-Era Retrospective Analysis for Research and Applications (MERRA) [*Rienecker et al.*, 2011] and the nudging approach is described in *Kunz et al.* [2011]. The QBO circulation is inherent in the MERRA meteorological fields and is therefore synchronized with that in the âĂIJrealâĂİ atmosphere. The horizontal resolution is the same as the pre-industrial simulation and the vertical resolution follows the MERRA reanalysis up to 50km. The lower stratosphere ranges from 1 km near the tropopause to about 2 km near the stratopause. The meteorological fields are nudged from the surface to 50 km; above 60 km the model meteorological fields are fully interactive, with a linear transition in between. Both versions of WACCM used in this study contain an identical representation of tropospheric and stratospheric chemistry [*Kinnison et al.*, 2007; *Tilmes et al.*, 2016]. The species included within this mechanism are contained within the Ox, NOx, HOx, ClOx, and BrOx chemical families, along with CH4 and its degradation products. In addition, 20 primary non-methane hydrocarbons and related oxygenated organic compounds are represented along with their surface emissions. There is a total of 183 species and 472 chemical reactions; this includes 17 heterogeneous reactions on multiple aerosol types (i.e., sulfate, nitric acid trihydrate, and water-ice).

From the aforementioned simulations, daily climatologies of zonal-mean ozone were constructed for the "preindustrial" (PI) years 1850-1860 and "ozone-hole" (OH) years 1995-2001, and smoothed to remove temporal variability on scales shorter than 10 days. For each latitude, height, and day, the ozone from the E2.1 control run was multiplied by the ratio OH/PI, with a small adjustment to preserve the vertical integral of OH-PI. Due to inter-model differences in PI ozone climatology, direct use of the absolute ozone amounts from OH would have introduced responses unrelated to the OH-PI ozone change; specification of that change in (multiplicative) anomaly form isolates the desired signal.

Figure S1

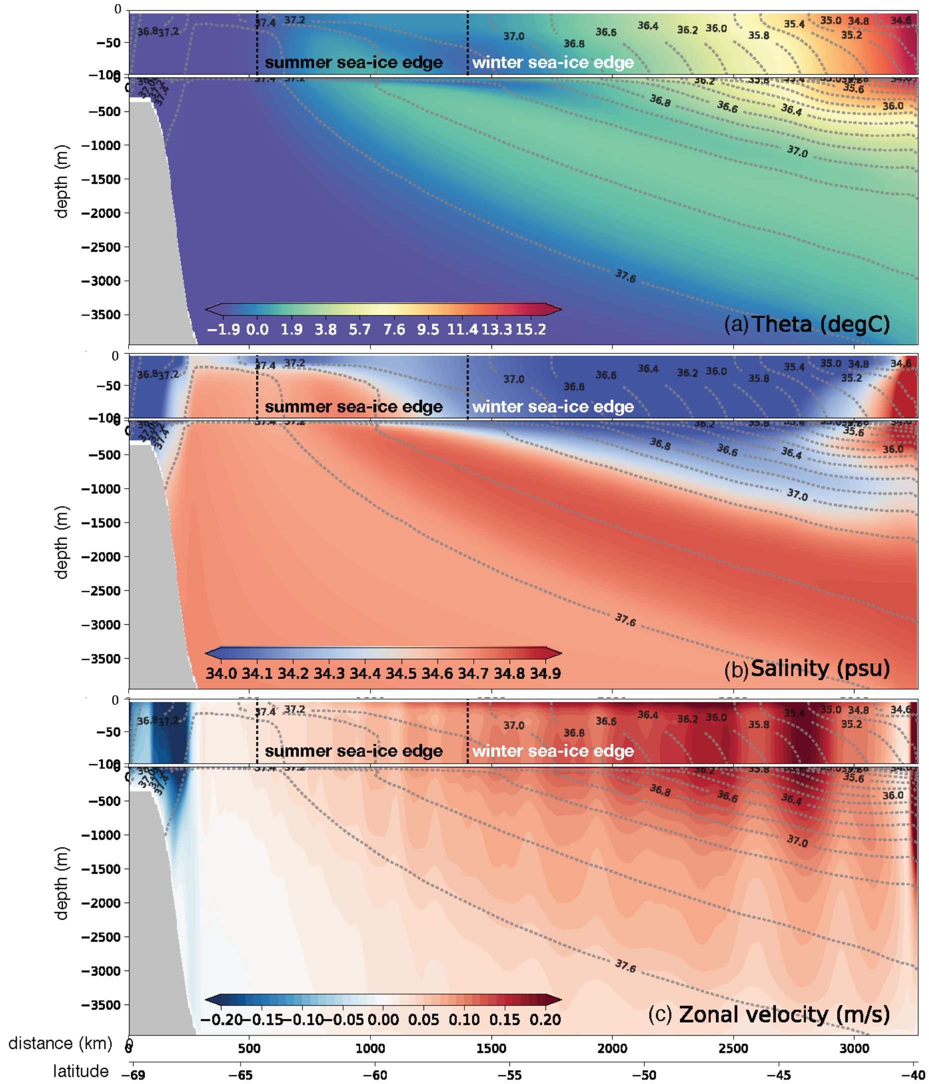

Figure S1: Annual mean (a) temperature, (b) salinity and (c) zonal velocity are plotted in shadings. The annual mean zonal wind stress (τ_x) is also plotted on top of (a). Gray contours are potential density referenced at 2000 m, (σ_2).

Figure S2

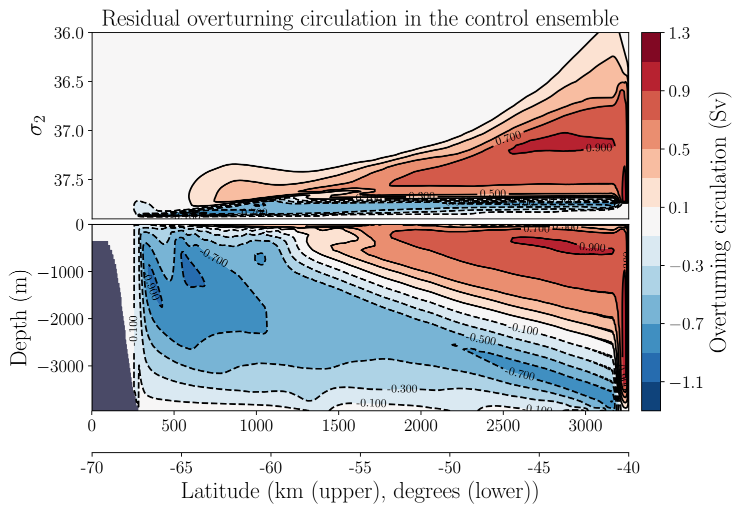

Figure S2: Residual overturning circulation in σ_2 and and depth coordinates.

Figure S3

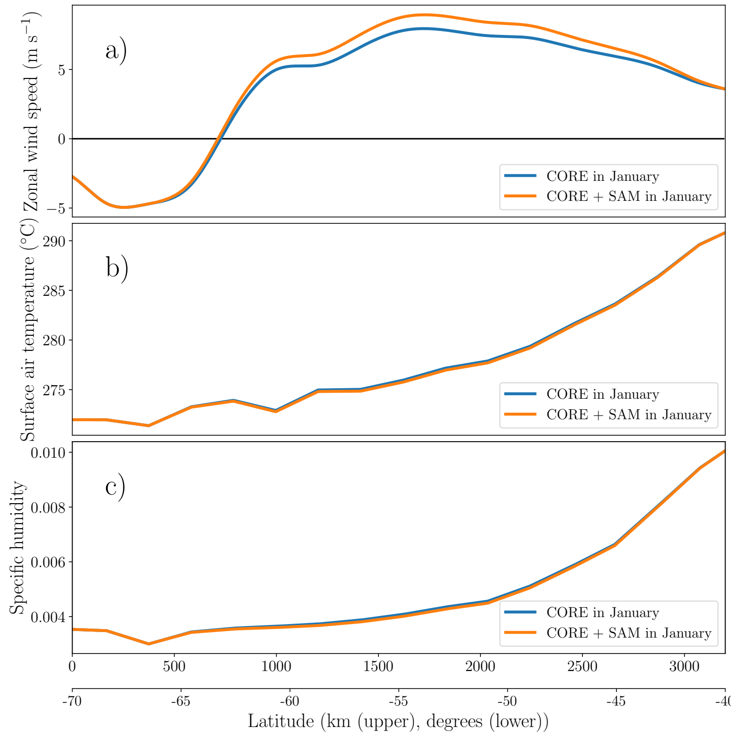

Figure S3: Atmospheric forcing fields extracted from the CORE normal year forcing set. a) zonal wind speed b) surface air temperature c) specific humidity. All fields and perturbations are from January. The surface temperature and specific humidity anomalies are small enough that the lines largely plot over the top of each other.

References

Adcroft, A. J., C. Hill, and J. C. Marshall (1997), Representation of Topography by Shaved Cells in a Height Coordinate Ocean Model, *Mon. Weather Rev.*, *125*, 2293–2315, doi:10.1175/1520-0493(1997)125<2293:ROTBSC>2.0.CO;2.

Garcia, R. R., D. R. Marsh, D. E. Kinnison, B. A. Boville, and F. Sassi (2007), Simulation of secular trends in the middle atmosphere, 1950-2003, *J. Geophys. Res. Atmos.*, *112*(9), 1–23, doi:10.1029/2006JD007485.

Garcia, R. R., A. K. Smith, D. E. Kinnison, Á. de la Cámara, and D. J. Murphy (2017), Modification of the Gravity Wave Parameterization in the Whole Atmosphere Community Climate Model: Motivation and Results, *J. Atmos. Sci.*, *74*(1), 275–291, doi:10.1175/JAS-D-16-0104.1.

Gaspar, P., Y. Grégoris, and J.-M. Lefevre (1990), A simple eddy kinetic energy model for simulations of the oceanic vertical mixing: Tests at station Papa and long-term upper ocean study site, *J. Geophys. Res.*, *95*(C9), 16,179, doi:10.1029/JC095iC09p16179.

Gent, P. R., and J. C. Mcwilliams (1990), Isopycnal Mixing in Ocean Circulation Models, *J. Phys. Oceanogr.*, *20*(1), 150–155, doi:10.1175/1520-0485(1990)020<0150:IMIOCM>2.0.CO;2.

Gent, P. R., J. Willebrand, T. J. McDougall, and J. C. McWilliams (1995), Parameterizing Eddy-Induced Tracer Transports in Ocean Circulation Models, *J. Phys. Oceanogr.*, *25*(4), 463–474, doi:10.1175/1520-0485(1995)025<0463:PEITTI>2.0.CO;2.

Hunke, E. C., and J. K. Dukowicz (1997), An ElasticâĂŞViscousâĂŞPlastic Model for Sea Ice Dynamics, *J. Phys. Oceanogr.*, *27*(9), 1849–1867, doi:10.1175/1520-0485(1997)027<1849:AEVPMF>2.0.CO;2.

Kinnison, D. E., G. P. Brasseur, S. Walters, R. R. Garcia, D. R. Marsh, F. Sassi, V. L. Harvey, C. E. Randall, L. Emmons, J. F. Lamarque, P. Hess, J. J. Orlando, X. X. Tie, W. Randel, L. L. Pan, A. Gettelman, C. Granier, T. Diehl, U. Niemeier, and A. J. Simmons (2007), Sensitivity of chemical tracers to meteorological parameters in the MOZART-3 chemical transport model, *J. Geophys. Res. Atmos.*, *112*(20), 1–24, doi:10.1029/2006JD007879.

Kunz, A., L. L. Pan, P. Konopka, D. E. Kinnison, and S. Tilmes (2011), Chemical and dynamical discontinuity at the extratropical tropopause based on START08 and WACCM analyses, *J. Geophys. Res. Atmos.*, *116*(24), 1–15, doi:10.1029/2011JD016686.

Lamarque, J. F., L. K. Emmons, P. G. Hess, D. E. Kinnison, S. Tilmes, F. Vitt, C. L. Heald, E. A. Holland, P. H. Lauritzen, J. Neu, J. J. Orlando, P. J. Rasch, and G. K. Tyndall (2012), CAM-chem: Description and evaluation of interactive atmospheric chemistry in the Community Earth System Model, *Geosci. Model Dev.*, *5*(2), 369–411, doi: 10.5194/gmd-5-369-2012.

Large, W. G., and S. Pond (1982), Sensible and Latent Heat Flux Measurements over the Ocean, doi:10.1175/1520-0485(1982)012<0464:SALHFM>2.0.CO;2.

Large, W. G., and S. G. Yeager (2009), The global climatology of an interannually varying air - Sea flux data set, *Clim. Dyn.*, *33*(2-3), 341–364, doi:10.1007/s00382-008-0441-3.

Lin, S.-J. (2004), A âĂIJVertically LagrangianâĂİ Finite-Volume Dynamical Core for Global Models, *Mon. Weather Rev.*, *132*(10), 2293–2307, doi:10.1175/1520-0493(2004)132<2293:AVLFDC>2.0.CO;2.

Locarnini, R. A., A. V. Mishonov, J. I. Antonov, T. P. Boyer, H. E. Garcia, O. K. Baranova, M. M. Zweng, C. R. Paver, J. R. Reagan, D. R. Johnson, M. Hamilton, and D. Seidov (2013), World Ocean Atlas 2013, Volume 1: Temperature, *Tech. rep.*

Losch, M., D. Menemenlis, J. M. Campin, P. Heimbach, and C. Hill (2010), On the formulation of sea-ice models. Part 1: Effects of different solver implementations and parameterizations, *Ocean Model.*, *33*(1-2), 129–144, doi:10.1016/j.ocemod.2009.12.008.

Marsh, D. R., M. J. Mills, D. E. Kinnison, J. F. Lamarque, N. Calvo, and L. M. Polvani (2013), Climate change from 1850 to 2005 simulated in CESM1(WACCM), *J. Clim.*, *26*(19), 7372–7391, doi:10.1175/JCLI-D-12-00558.1.

Marshall, J., C. Hill, L. Perelman, and A. Adcroft (1997a), Hydrostatic, quasi-hydrostatic, and nonhydrostatic ocean modeling, *J. Geophys. Res. Ocean.*, *102*(C3), 5733–5752, doi: 10.1029/96JC02776.

Marshall, J., H. Jones, and C. Hill (1998), Efficient ocean modeling using non-hydrostatic algorithms, *J. Mar. Syst.*, *18*(1-3), 115–134, doi:10.1016/S0924-7963(98)00008-6.

Marshall, J. C., A. Adcroft, C. Hill, L. Perelman, and C. Heisey (1997b), A finite-volume, incompressible Navier Stokes model for studies of the ocean on parallel computers, *J. Geophys. Res. Ocean.*, *102*(C3), 5753–5766, doi:10.1029/96JC02775.

Morgenstern, O., M. Hegglin, E. Rozanov, F. O'Connor, N. Luke Abraham, H. Akiyoshi, A. Archibald, S. Bekki, N. Butchart, M. Chipperfield, M. Deushi, S. Dhomse, R. Garcia, S. Hardiman, L. Horowitz, P. Jöckel, B. Josse, D. Kinnison, M. Lin, E. Mancini, M. Manyin, M. Marchand, V. Marécal, M. Michou, L. Oman, G. Pitari, D. Plummer,

L. Revell, D. Saint-Martin, R. Schofield, A. Stenke, K. Stone, K. Sudo, T. Tanaka, S. Tilmes, Y. Yamashita, K. Yoshida, and G. Zeng (2017), Review of the global models used within phase 1 of the Chemistry-Climate Model Initiative (CCMI), *Geosci. Model Dev.*, *10*(2), 639–671, doi:10.5194/gmd-10-639-2017.

Neale, R. B., J. Richter, S. Park, P. H. Lauritzen, S. J. Vavrus, P. J. Rasch, and M. Zhang (2013), The Mean Climate of the Community Atmosphere Model (CAM4) in Forced SST and Fully Coupled Experiments, *J. Clim.*, *26*(14), 5150–5168, doi:10.1175/JCLI-D-12-00236.1.

Redi, M. H. (1982), Oceanic Isopycnal Mixing by Coordinate Rotation, *J. Phys. Oceanogr.*, *12*(10), 1154–1158, doi:10.1175/1520-0485(1982)012<1154:OIMBCR>2.0.CO;2.

Rienecker, M. M., M. J. Suarez, R. Gelaro, R. Todling, J. Bacmeister, E. Liu, M. G. Bosilovich, S. D. Schubert, L. Takacs, G. K. Kim, S. Bloom, J. Chen, D. Collins, A. Conaty, A. Da Silva, W. Gu, J. Joiner, R. D. Koster, R. Lucchesi, A. Molod, T. Owens, S. Pawson, P. Pegion, C. R. Redder, R. Reichle, F. R. Robertson, A. G. Ruddick, M. Sienkiewicz, and J. Woollen (2011), MERRA: NASA's modern-era retrospective analysis for research and applications, *J. Clim.*, *24*(14), 3624–3648, doi:10.1175/JCLI-D-11-00015.1.

Schmidt, G. A., M. Kelley, L. Nazarenko, R. Ruedy, G. L. Russell, I. Aleinov, M. Bauer, S. E. Bauer, M. K. Bhat, R. Bleck, V. Canuto, Y.-h. Chen, Y. Cheng, T. L. Clune, A. D. Genio, R. D. Fainchtein, G. Faluvegi, J. E. Hansen, R. J. Healy, N. Y. Kiang, D. Koch, A. A. Lacis, A. N. Legrande, J. Lerner, K. K. Lo, E. E. Matthews, S. Menon, R. L. Miller, V. Oinas, and A. O. Oloso (2014), Journal of Advances in Modeling Earth Systems contributions to the CMIP5 archive, *J. Adv. Model. Earth Syst.*, *6*, 141–184, doi:10.1002/2013MS000265.Received.

Solomon, S., D. Kinnison, J. Bandoro, and R. Garcia (2015), Simulation of polar ozone depletion: An update, *J. Geophys. Res.*, *120*(15), 7958–7974, doi:10.1002/2015JD023365.

Tilmes, S., J. F. Lamarque, L. K. Emmons, D. E. Kinnison, D. Marsh, R. R. Garcia, A. K. Smith, R. R. Neely, A. Conley, F. Vitt, M. Val Martin, H. Tanimoto, I. Simpson, D. R. Blake, and N. Blake (2016), Representation of the Community Earth System Model (CESM1) CAM4-chem within the Chemistry-Climate Model Initiative (CCMI), *Geosci. Model Dev.*, *9*(5), 1853–1890, doi:10.5194/gmd-9-1853-2016.

Visbeck, M., J. Marshall, T. Haine, and M. Spall (1997), Specification of Eddy Transfer Coefficients in Coarse-Resolution Ocean Circulation Models*, *J. Phys. Oceanogr.*, *27*(3), 381–402, doi:10.1175/1520-0485(1997)027<0381:SOETCI>2.0.CO;2.

Winton, M. (2000), A reformulated three-layer sea ice model, *J. Atmos. Ocean. Technol.*, *17*(4), 525–531, doi:10.1175/1520-0426(2000)017<0525:ARTLSI>2.0.CO;2.

Zweng, M. M., J. R. Reagan, J. I. Antonov, R. A. Locarnini, A. V. Mishonov, T. P. Boyer, H. E. Garcia, O. K. Baranova, D. R. Johnson, D.Seidov, and M. M. Biddle (2013), Salinity, in *World Ocean Atlas 2013*, *74*, vol. 2, edited by S. Levitus, p. 39, NOAA Atlas NESDIS.